Bombarding-energy dependence of the $^{209}Bi + ^{136}Xe$ reaction

W. W. Wilcke, J. R. Birkelund, A. D. Hoover, J. R. Huizenga, and W. U. Schröder
Departments of Chemistry and Physics and Nuclear Structure Research Laboratory, University of Rochester, Rochester, New York 14627

V. E. Viola, Jr.
Department of Chemistry, University of Maryland, College Park, Maryland 20742

K. L. Wolf and A. C. Mignerey
Argonne National Laboratory, Argonne, Illinois 60439

(Received 11 January 1980)

A previous study of the strongly damped reaction $^{209}Bi + ^{136}Xe$ at 1130 MeV has been extended to the lower bombarding energy of 940 MeV. With the same experimental technique, angular, energy, and atomic charge distributions and their correlations have been measured. The angular distribution of the reaction products is sideways peaked, but less strongly focused than at the higher bombarding energy. The energy spectrum extends far below the Coulomb energy calculated for touching spherical ions, indicating large deformations of the final fragments. The charge distributions are Gaussians approximately centered around the initial fragmentation. Examination of the correlations between experimental observables confirms that the energy-loss parameter is the most suitable quantity to describe the time evolution of the reaction. The relationship between energy loss and the width of the charge distribution is studied to gain information on the contribution of the nucleon exchange process to the total dissipated energy. The bombarding-energy dependence of this relationship suggests that the Pauli blocking of occupied single particle levels is an important effect, leading to a smaller dispersion of the fragment Z distribution for a given energy loss than expected from a classical theory. A quantitative analysis establishes the nucleon exchange as the dominant mechanism for the dissipation of kinetic energy. With the aid of a phenomenological model, a decomposition of the reaction cross section in partial waves is performed. Classical trajectory calculations assuming spherical ions are compared to an empirically determined deflection function, energy loss, and interaction times. These calculations do not provide a consistent description of the experimental results, since the energy loss is systematically underestimated. From the interaction times and widths of the charge distributions, an angular momentum dependent proton number diffusion coefficient $D_Z(l)$ is derived, which shows a pronounced saturation behavior for angular momenta less than 2/3 of the grazing angular momentum. The total probability for sequential fission of the targetlike fragment is determined to be 30% for all inelastic events. A simple model is presented which allows calculation of this probability on the basis of known fission properties of heavy elements.

[NUCLEAR REACTIONS $^{209}Bi + ^{136}Xe$, $E_{lab} = 940$ MeV; measured $\sigma(\theta, E, Z)$; strongly damped reaction; deduced correlations, interaction times, transport coefficients; comparison to trajectory calculations; yield of sequential fission.]

I. INTRODUCTION

The reaction $^{209}Bi + ^{136}Xe$ has been studied previously[1] at a bombarding energy of $E_{lab} = 1130$ MeV as a typical example of a strongly damped reaction. The use of such a heavy system has several advantages. Strongly damped collisions are by far the dominant reaction mechanism and allow, therefore, the study of the reaction over a wide range of impact parameters, from grazing collisions to nearly central impacts. Thus the correlations between observable quantities such as dissipated kinetic energy, reaction angle, and the charge distribution of the final reaction fragments can be studied much more readily than for light systems, where only a comparatively narrow window of impact parameters leads to strongly damped events.[2]

It has been shown in the previous study,[1] that the degree of kinetic energy dissipation is the most useful parameter to characterize the time development of strongly damped reactions. Therefore, it is a natural extension of this investigation to change the bombarding energy and thus the amount of kinetic energy available for dissipation. This paper reports on a detailed study of the system $^{209}Bi + ^{136}Xe$ at a bombarding energy of $E_{lab} = 940$ MeV, an energy of 1.4 times the Coulomb energy of touching spheres.

In the following section, the experimental procedures are described briefly. Results on elastic scattering, angular, charge, and energy distributions for the Xe- and Bi-like reaction products are discussed in Sec. III. In Sec. IV the implications of the experimental results for the understanding

of the reaction mechanism are discussed. Special attention is given to the importance of nucleon exchange as a mechanism of energy dissipation and to the importance of the Pauli principle for an understanding of the correlation between the widths of the element distributions and the degree of energy damping. In Sec. V a model is presented to calculate the observed yield of sequential fission of the Bi-like fragments. A summary can be found in Sec. VI.

II. EXPERIMENTAL PROCEDURE AND DATA REDUCTION

The experiments were performed at the LBL SuperHILAC accelerator. Targets of 235 $\mu g/cm^2$ ^{209}Bi on carbon backings were bombarded with 940-MeV ^{136}Xe ions. The beam energy was determined with four independent detector systems calibrated with α and ^{252}Cf fission sources. The result was 940 MeV, with a statistical uncertainity of 12 MeV, allowing for a pulse height defect of 51 MeV according to the procedure of Moulton *et al.*[3-5] The reaction products were detected in two ΔE-E silicon surface barrier detector telescopes and one silicon detector. The thicknesses of the two ΔE detectors were 14.3 and 9.6 μm, respectively. The telescopes subtended angles of 0.5° and 1.0° in the reaction plane. Two monitor counters, placed out of plane at fixed forward angles monitored the beam intensity and allowed for dead-time corrections. The beam was defined by two pairs of slits outside the chamber and one pair of cleanup slits at its entrance. Permanent magnets and 160 $\mu g/cm^2$ thick Ni foils protected the detectors from delta electrons generated by the beam.

The electronic setup was very similar to the one described in Ref. 1, and included pileup circuitry and a system allowing a determination of the system dead time, taking into account the pulsed character of the HILAC beam. All data were recorded on magnetic tape in an event-by-event mode.

In Fig. 1 are shown examples of the laboratory energy spectra taken with the singles detector. The spectrum at $\theta_L = 24°$ shows an intense elastic peak at 838 MeV, a broad bump of strongly damped events centered at 600 MeV, and a second small bump at 450 MeV which is due to sequential fission of the heavy, Bi-like fragments, which are also scattered to forward angles for large negative reaction Q values. In the two-dimensional ΔE-E spectra the two groups of fragments are well separated.

At $\theta_L = 38°$ the elastic peak is still dominant and has a low-energy tail smoothly joining the strongly damped, Xe-like fragments centered around 550 MeV. The Bi-like fragments show up at this angle

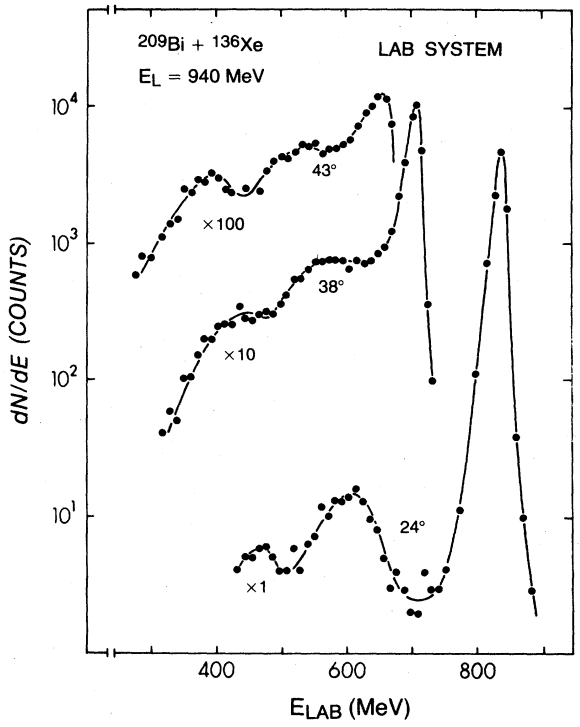

FIG. 1. Laboratory energy spectra of the reaction products taken at the angles indicated.

as a bump located around 420 MeV, whereas the sequential fission events are not distinguishable from other events in the one-dimensional spectrum. At $\theta_L = 43°$, very close to the quarter-point angle, the spectrum shows the same components as at $\theta_L = 38°$. For larger angles the spectra are dominated by the recoil nuclei.

Since elastic scattering events were not resolved from those with small energy losses, a standard peak was defined at forward scattering angles and subtracted from the spectra taken at angles in the vicinity of the quarter point. This procedure has been used extensively in the analysis of heavy ion elastic scattering.[6]

The experimental ΔE-E distributions were converted into Z-E distributions using the tables of Northcliffe and Schilling,[7] renormalized to the experimental stopping power of Xe ions in Si. A constant mass-to-charge ratio of $A/Z = 2.52$ was assumed to convert the measured fragment charge into fragment mass, necessary to perform kinematical calculations. Since ^{136}Xe and ^{209}Bi both have this mass-to-charge ratio, no change in the A/Z ratio is expected to occur during the interaction. The Z-E distributions were transformed into the center-of-mass system for 26-MeV-wide bins of the asymtotically measured center-of-mass total kinetic energy E, using the experimentally established fact that strongly damped reactions at low

bombarding energies are essentially of a binary nature,[2] except for light-particle evaporation from the highly excited fragments. The reduction in kinetic energy of the fragments in the laboratory system due to the evaporation of neutrons was corrected for. Details of this calculation can be found in Ref. 1. Further corrections were applied for the energy loss in the target and Ni foils and for the pulse-height defect in the detectors.

For angles up to the quarter point, the heavy, Bi-like fragments could easily be distinguished from the light fragments, because they occupy a well defined region in the Z-E plane. For larger angles, Xe-like fragments with very large Z transfer merge with the Bi-like fragments, and the separation between the fragments is not quite as unambiguous. However, the uncertainty in the reaction cross section introduced by this overlap is not large. Since a sizable fraction of the heavy fragments is expected to undergo sequential fission, the yield of Bi-like reaction products is of interest. Because there is no simple way to discriminate the elastic recoil events from heavy reaction products, due to insufficient Z and E resolution, the elastic recoils were accounted for by determining the cross section of elastically scattered Bi from the measured Xe angular distribution and subtracting it from the total yield of heavy fragments.

III. EXPERIMENTAL RESULTS AND DISCUSSION

A. Elastic scattering and the reaction cross section

The elastic scattering was investigated in order to obtain information on the bombarding-energy dependence of the total reaction cross section σ_R, the strong absorption radius R_{SA}, and an optical-model potential suitable to describe the scattering.

Figure 2 shows the ratio of elastic-to-Rutherford cross section in the center-of-mass system. Compared to the experiment at 1130-MeV bombarding energy, the quarter-point angle is shifted backwards to $\theta_{c.m.} = 70.1°$, and the slope of the angular distribution at the quarter point is smaller.

The data were analyzed using two models: the semiquantal model of Fresnel scattering[8] and a one-channel optical model. The reaction parameters deduced are compiled in Table I. In a simple version of the Fresnel model the transmission coefficients are approximated by a step function: $T_l = 1$ for $l \leq l_g$ and $T_l = 0$ for $l > l_g$, where l_g represents the grazing angular momentum. Since this sharp-cutoff model is known to produce large oscillations of the ratio $d\sigma_{el}/d\sigma_{Ruth}$ forward of the quarter-point angle, it was refined[9] by introducing a finite transition region in l space of width Δl. The broken curve in Fig. 2 indicates the prediction

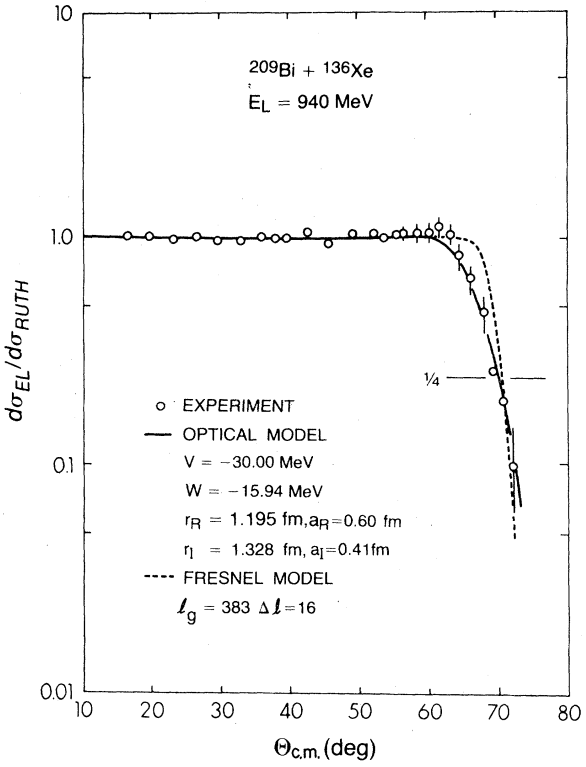

FIG. 2. The experimental ratio $d\sigma_{el}/d\sigma_{Ruth}$ of the elastic-to-Rutherford cross section as a function of the center-of-mass scattering angle is compared to calculations using the generalized Fresnel model (dashed curve) and an optical model (solid curve).

of this model for $\Delta l = 16$. Although the overall agreement with the data is reasonable, the relatively gradual falloff of the data cannot be reproduced by the Fresnel model, regardless of the

TABLE I. A comparison of the reaction parameter for the system ^{209}Bi + ^{136}Xe at two bombarding energies.

Quantity	940 MeV	1130 MeV	Units
E_{lab}	940	1130	MeV
$E_{c.m.}$	569	684	MeV
$\theta_{1/4}$ (lab)	43.5°	33°	deg
$\theta_{1/4}$ (c.m.)	70.1°	54°	deg
μ (reduced mass)	82.4	82.4	u
k_∞ (wave number)	47.37	51.94	fm^{-1}
η (Coulomb parameter)	268.4	244.8	
R_{int} (Fresnel)	15.5	15.1	fm
l_g (Fresnel exp $\theta_{1/4}$)	383	480	$\hbar$
σ_R (Fresnel exp $\theta_{1/4}$)	2.06	2.70	b
σ_R (exp)	2.09	2.80	b
R_{SA} (optical model)	15.5	15.2	fm
V_C (R_{int})	416	428	MeV
$T_0 = E_{c.m.} - V_C(R_{int})$	152	256	MeV
$[E_{c.m.} - V_C(R_{int})]/\mu$	1.86	3.11	MeV/u
Peak in $d\sigma_R/d\Omega$ (lab)	39.5°	30°	deg
Peak in (c.m.)	64.5°	50°	deg

width Δl chosen. It is not too surprising that the Fresnel model does not fit the present experimental data at 940 MeV as well as the data taken at 1130 MeV, because it is known[8] that diffractive models lose their validity for bombarding energies close to the Coulomb barrier.

Nevertheless, the present experiment still allows extraction of a meaningful value for the grazing angular momentum l_g, where the transmission coefficient assumes the value $\frac{3}{4}$, via the relation

$$\theta_{1/4} = 2 \arctan[\eta/(l_g + \tfrac{1}{2})] \tag{3.1}$$

and of the total reaction cross section

$$\sigma_R = \frac{\pi}{k^2}(l_g + \tfrac{1}{2})^2 \left[1 + 2\frac{\Delta l}{l_g + \frac{1}{2}} + \frac{\pi^2}{3}\left(\frac{\Delta l}{l_g + \frac{1}{2}}\right)^2\right]. \tag{3.2}$$

Here, η is the Coulomb parameter and k the asymptotic wave number. The values obtained are $l_g = 383$ and $\sigma_R = 2.2$ b, very similar to the results derived from the simple version of the Fresnel model ($l_g = 383, \sigma_R = 2.1$ b). From these values an interaction radius of $R_{\text{int}} = 15.5$ fm is deduced. This radius is slightly larger than that deduced for the same system at 1130-MeV bombarding energy (15.1 fm). An optical-model calculation was performed to check the dependence of the deduced interaction radius on the type of analysis made. A standard Woods-Saxon nuclear potential was used to generate the elastic angular distributions with the optical-model code GENOA.[10]

A set of parameters which fit the 1130-MeV data very well produced results which missed the experimental quarter point by several degrees. A two-parameter search on the radii determined values which are considerably larger than the starting values. The strong absorption radius R_{SA} defined by

$$kR_{\text{SA}} = \eta + [\eta^2 + l_g(l_g + 1)]^{1/2} \tag{3.3}$$

was found to be 15.5 fm, which is consistent with an increase of the interaction radius at the lower bombarding energy. There is some confirmation of this tendency from other analyses of heavy ion elastic scattering.[6,11]

These findings illuminate the well known difficulty in defining a unique and energy independent optical potential for very heavy ion reactions. Therefore, no further attempt was made to search for a set of more suitable optical-model parameters. For the further analysis the grazing angular momentum as extracted with the modified Fresnel model was employed in order to be consistent with Ref. 1.

B. Angular, charge, and energy distributions of the Xe-like reaction fragments

The angular distribution of the light reaction products in the laboratory system is shown in Fig. 3. Similar to the 1130-MeV experiment, the cross section is focused around an angle slightly forward of the quarter-point angle. The integration of the data yields an experimental total reaction cross section of $\sigma_R = (2.1 \pm 0.1)$ b, in good agreement with the analysis of the elastic scattering data. Towards forward and backward angles the cross section drops quickly, and the data are consistent with vanishing cross section at $\theta = 0°$, indicating that no negative-angle scattering (orbiting) occurs. This is not surprising since orbiting should become less pronounced with decreasing bombarding energy and increasing product $Z_P \cdot Z_T$.[2,12]

In Fig. 4 the angular distribution is shown in the center-of-mass system for all events with a total kinetic energy E between 260 and 546 MeV. Since elastic scattering corresponds to an energy of 569 MeV, most of the quasielastic events have been excluded. Compared to the 1130-MeV experiment, the angular distribution is skewed and extends further backwards, indicating that the nearly perfect angular focusing at 1130 MeV is not an intrinsic feature of the reaction ^{209}Bi + ^{136}Xe, but has to be viewed as the coincidental result of a delicate balence between nuclear, Coulomb, and centrifugal forces, which is destroyed at other bombarding energies.

The Z distribution of the Xe-like fragments is shown in Fig. 5, integrated over the same range of total kinetic energies. The weak asymmetry is due to a slight shift of the centroid of the Z distribution towards higher Z for decreasing energies. The bump around $Z = 41$ is caused by a weak contamination with sequential-fission products of Bi-like

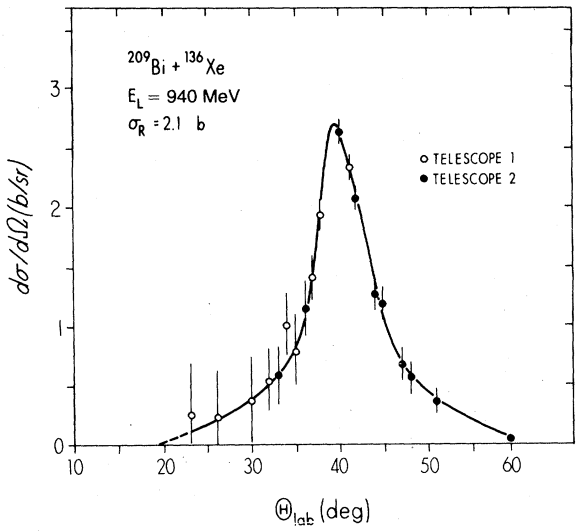

FIG. 3. Laboratory angular distribution of the light, Xe-like reaction products. The curve is to guide the eye.

TABLE II. The angular distribution of the Xe-like fragments in the c.m. system, integrated over all Z and all E values between 260 and 545 MeV. This accounts for 80% of the reaction cross section. The unit of the table entries is mb/sr.

	+0°	+1°	+2°	+3°	+4°	+5°	+6°	+7°	+8°	+9°
40°					10	15	22	25	28	33
50°	39	52	65	74	94	126	159	178	182	200
60°	317	408	505	865	1046	1033	994	921	859	783
70°	760	655	617	556	489	438	386	348	309	276
80°	256	240	231	203	172	164	159	158	149	130
90°	121	112	93	73	61	50	42	37	30	25

fragments, which could not be separated completely from the highly damped events. The correlation of the Z distribution with the energy-loss parameter will be discussed later.

In Fig. 6 the energy-loss spectrum is shown for the two bombarding energies under study. The arrows indicate the initially available kinetic energies above the Coulomb barrier as calculated assuming spherical ions separated by the strong interaction radius. The data show clearly that a large fraction of the reaction cross section cannot be explained without assuming strong deformations of the fragments at the time of breakup. This is especially important at the low bombarding energy where 800 mb (or 40%) of the total reaction cross section corresponds to final kinetic energies below the Coulomb barrier, as compared to 500 mb (or 20%) for the 1130-MeV experiment.

It should be pointed out that the cross section for very low-energy losses (below 20 MeV) is not very well known due to insufficient experimental energy resolution. It was not possible to determine whether the cross section rises monotonically in the quasielastic region, or reaches a maximum around 10-MeV energy loss. In the present paper, a monotonic increase of $d\sigma/dE_{\text{loss}}$ with decreasing energy loss has been assumed in the quasielastic region.

C. Angular distribution of the Bi-like fragments

In contrast to the experiment at 1130 MeV, it was possible in the present experiment to observe the heavy Bi-like fragments simultaneously with the light fragments over a wide angular range. The heavy fragments appear as a well separated island in the ΔE vs E distributions for all but the largest angles, where the fringes of the light and heavy fragment Z distribution start to overlap. It was not possible to make a reliable Z identification for the slow Bi-like fragments and, therefore, no conversion into the center-of-mass system was performed. However, the angular distribution of the inelastically scattered heavy fragments was obtained indirectly. This was done by subtracting the number of elastically scattered Bi ions, as deter-

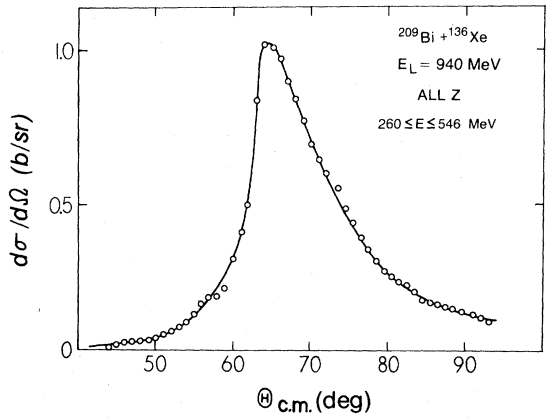

FIG. 4. Center-of-mass angular distribution of the reaction cross section for events with total kinetic energies in the indicated range. This distribution accounts for 80% of the total reaction cross section.

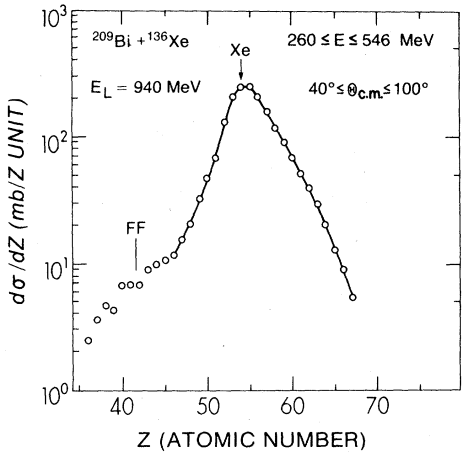

FIG. 5. The Z distribution of projectile-like fragments integrated over the indicated angle and TKE range. The low-Z wing of the distribution is slightly affected by incompletely removed events from sequential fission of the heavy fragment.

TABLE III. The charge distribution of the Xe-like fragments, integrated over angle 40° $\leq \theta_{c.m.} \leq$ 100°, and E values between 260 and 545 MeV. The units of the table entries are mb/Z unit. The (*) indicates contamination with sequential fission events.

Z	+0	+1	+2	+3	+4	+5	+6	+7	+8	+9
40	6*	6*	6*	8*	9*	9*	11	14	18	29
50	44	64	121	194	224	229	190	148	108	80
60	62	45	36	26	17	12	6	4	2	1

mined from the measured angular distribution of the Xe ions, from the total number of Bi-like fragments for a given angle.

The resulting angular distribution of the Bi-like reaction products in the laboratory system is shown in Fig. 7. The pronounced asymmetry is due to a kinematic effect. The light reaction fragments are strongly focused into a narrow angular region, but with rising energy loss the corresponding heavy fragments are scattered to smaller angles. The long tail towards forward angles is, therefore, due to very strongly damped events.

The integrated cross section of the Bi-like fragments is only (1.5 ± 0.4) b, which is 30% smaller than the reaction cross section deduced from the light fragments. This difference can be explained by subsequent fission of the Bi-like reaction fragments in 30% of all nonelastic events. A discussion of this number with respect to known fission properties of elements near Bi is deferred to Sec. V.

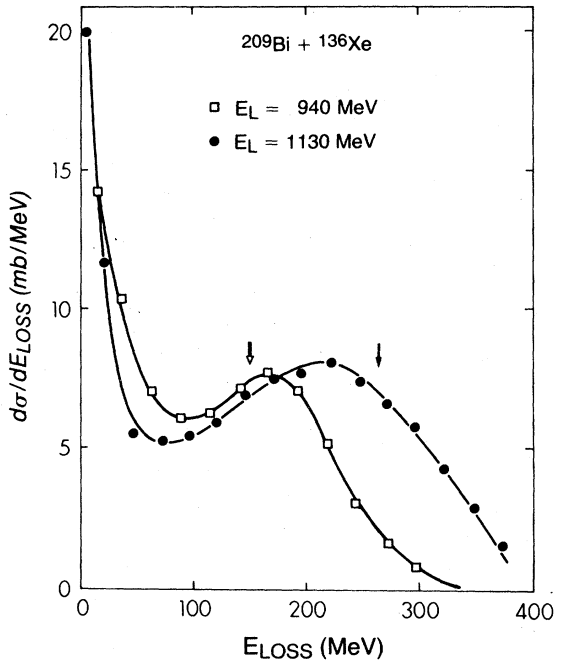

FIG. 6. The energy-loss spectrum of the ^{209}Bi+^{136}Xe reaction for 940- and 1130-MeV bombarding energy. The energy loss E_{loss} is defined as the difference between the center-of-mass asymptotic kinetic energies in the entrance and exit channels. The arrows indicate the available kinetic energy in the entrance channel.

D. Qualitative correlations of observables with fragment charge and kinetic energy loss

In Ref. 1 the importance of the energy-loss parameter $E_{loss} = E_{c.m.} - E$ is discussed in detail for the description of the strongly damped reaction between ^{136}Xe and ^{209}Bi at 1130 MeV. A knowledge of the energy loss determines the associated angular and Z distributions, whereas a selection of either Z or the scattering angle does not determine uniquely the other observables. This significance of the energy loss as a parameter characterizing the reaction is confirmed in the present experiment. In Fig. 8 the double-differential cross section $d^2\sigma/dZdE$ is plotted on a logarithmic scale versus the total kinetic energy of the fragments. The events are sorted into three-Z-unit-wide bins, the centroids of which are indicated at the spectra. The arrows indicate Coulomb energies calculated for spherical reaction products, assuming spheres touching at the strong absorption radius. It is obvious from Fig. 8 that multiple proton pickup and stripping reactions lead to rather similar energy-loss spectra, confirming that the charge of the light fragment is certainly not a suitable quantity

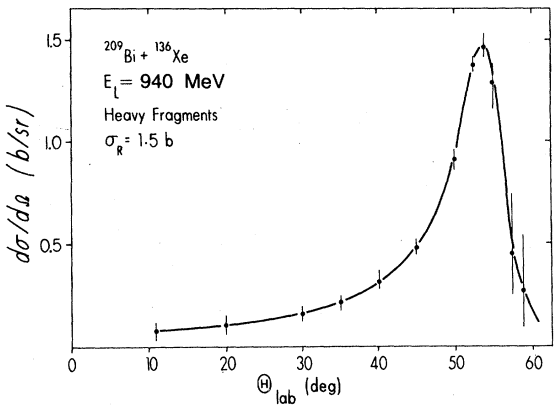

FIG. 7. Laboratory angular distribution of the heavy, target-like reaction products. The curve is intended to guide the eye.

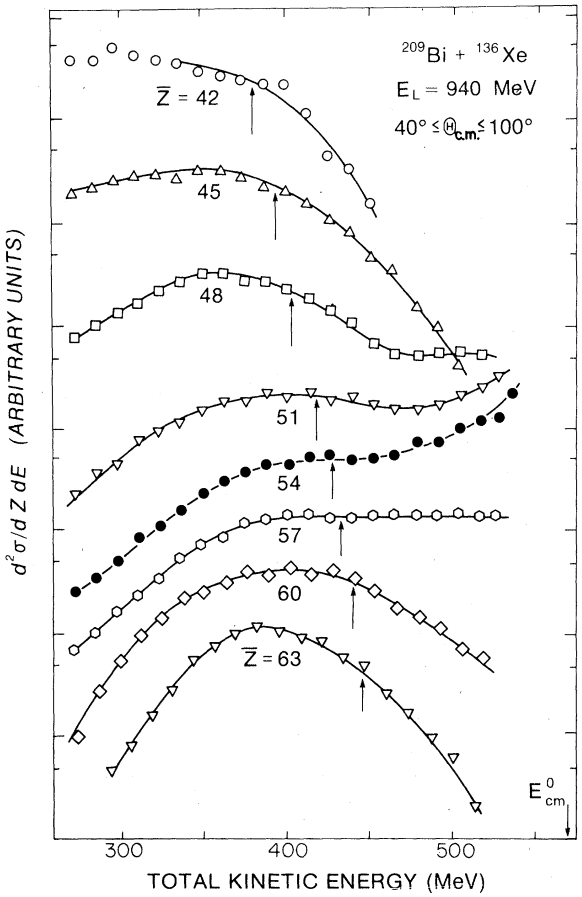

FIG. 8. Center-of-mass energy spectra for three Z-unit-wide bins. The centroid of each bin is indicated for each curve. The arrows represent Coulomb energies for spherical fragments. The curves are arbitrarily displaced along the ordinate.

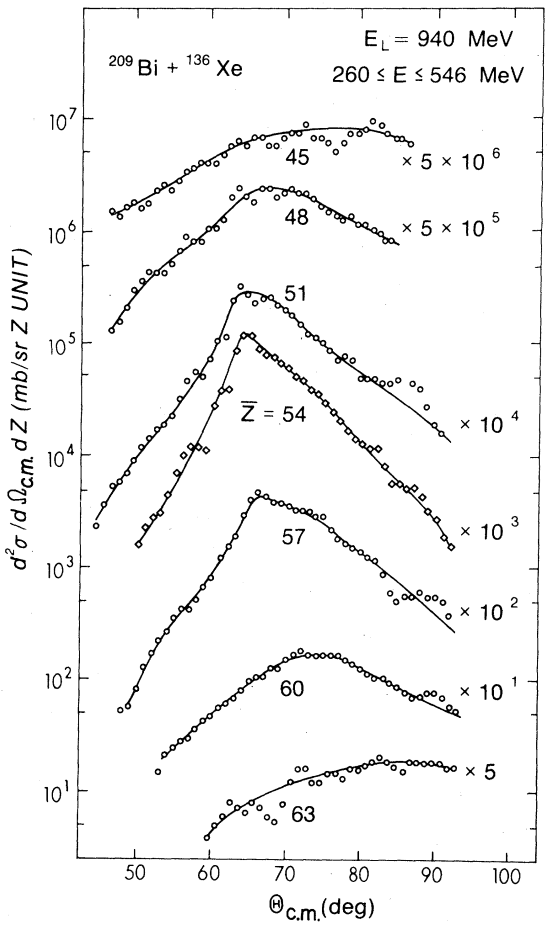

FIG. 9. Angular distribution of the damped reaction cross section as a function of the fragment Z.

to characterize a given strongly damped event. (The small difference in the shape of the spectra for the $\overline{Z}=42$ and the $\overline{Z}=63$ bins is at least partly due to the contamination of the former bin with sequential fission events.) A variation from the results of the experiment at 1130 MeV, however, is represented by the relative positions of the maxima in the spectra relative to the calculated Coulomb barriers. Whereas the maximum of the yield is always located at energies above the Coulomb barrier for $42 \leq Z \leq 63$ at 1130-MeV bombarding energy, this is a feature not corroborated for most Z bins in the present experiment. This emphasizes even more strongly the importance of considering deformations or neck degrees of freedom in understanding the low-energy data.

Similar to the energy-loss distributions, the angular distributions depend strongly on the atomic number of the fragment, but the correlation is not unique. This is shown in Fig. 9, where the double differential cross section $d^2\sigma/d\Omega_{\text{c.m.}}dZ$ is plotted for the same Z bins as in Fig. 8. The angular distributions of fragments near the projectile Z are strongly peaked, but the spectra for either very low or very high Z values of the light fragments look similar. In contrast to the findings obtained in the 1130-MeV experiment, the maxima of the angular distributions do not remain centered around $\theta_{\text{c.m.}} = 64°$, where the quasielastic cross section has a maximum, but are shifted steadily to larger angles with increasing magnitude of the charge transfer. A discussion of these results will be given in Sec. IV.

Since a large net charge transfer is related to a large energy loss, it is expected that the maxima in the double-differential cross section $d^2\sigma/d\Omega dE$ move to larger angles with increasing energy loss. This can indeed be seen in the Wilczyński plot[13] (Fig. 10), showing contour lines of the cross section in the E vs $\theta_{\text{c.m.}}$ plane. The ridge of damped events, starting out at $\theta_{\text{c.m.}} = 64°$, moves back-

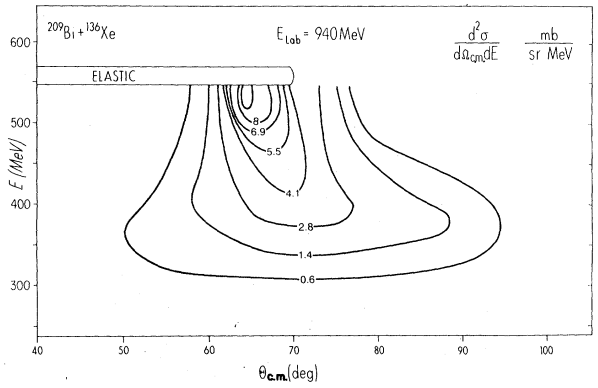

FIG. 10. Double-differential cross section $d^2\sigma/dEd\Omega$ plotted as a contour diagram (Wilczyński plot) in the TKE versus scattering-angle plane.

wards with decreasing E, whereas it was found to be parallel to the E axis in the 1130-MeV experiment. Qualitatively, this result is due to the lower angular momentum for a given impact parameter in the 940-MeV experiment. The Coulomb deflection towards backward angles is more pronounced, and the rotation towards forward angles during the nuclear interaction time is less for smaller angular momenta.

The angular distributions integrated over all Z for a given E bin, i.e., cuts of the Wilczyński plot parallel to the $\theta_{c.m.}$ axis, are shown in Fig. 11. The reaction cross section is sideways peaked for all E values, and no indication of orbiting, such as enhancement of the cross section at forward angles, is visible. The dominant feature of the angular distribution is the increase of its width with increasing energy loss, suggesting that longer reaction times are associated with higher energy losses.

The charge distributions $d^2\sigma/dEdZ$ of the Xe-like fragments as a function of the final total kinetic energy are shown in Fig. 12. It is obvious that the data can be described rather well by Gaussian distributions as indicated by the solid curves. The width of the Z distribution is seen to increase strongly with increasing energy loss, suggestive of a diffusion mechanism where the time available for the diffusion process increases monotonically with increasing energy loss.[14] The width of the 558-MeV bin is mostly due to the experimental Z resolution of about three Z units. The following analysis accounts for this intrinsic width by assuming an additive law of the variances σ_Z^2.

In agreement with the 1130-MeV experiment, the centroids of the charge distributions stay close to the charge of Xe and drift only very slowly towards mass symmetry. Experimental results for the cross section, the variance σ_Z^2, and the centroid

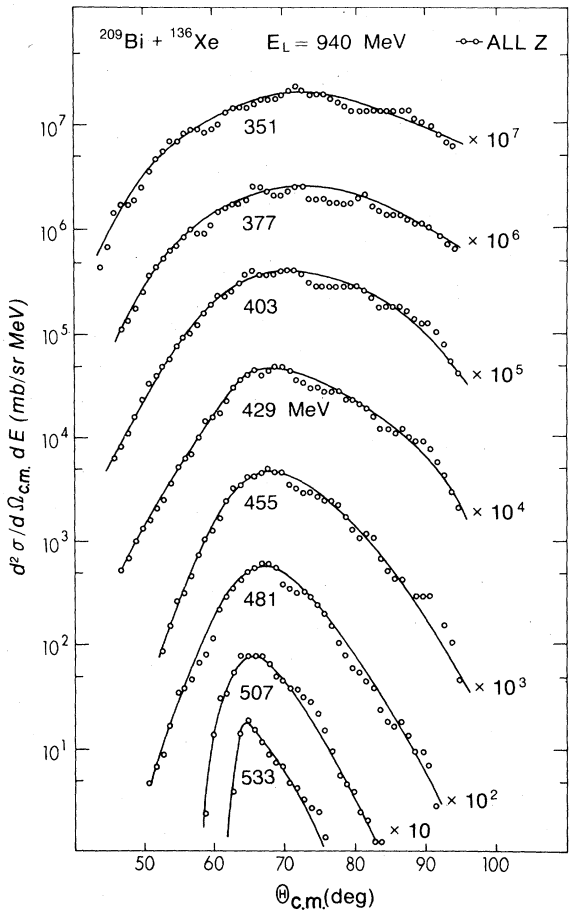

FIG. 11. Angular distribution for 26-MeV-wide TKE bins integrated over the Z range indicated. The centroid energy for each bin is given at each curve.

$\langle Z\rangle$ of the fragment charge distributions are collected in Table IV for 26-MeV-wide E bins.

The relationship between the variance σ_Z^2 and the energy loss is plotted in Fig. 13 for the two bombarding energies. For energy losses up to 100 MeV the two curves are indistinguishable within the experimental errors, but then the energy loss rises less fast for a given increase in σ_Z^2 at the lower bombarding energy. This is to be expected since there is much less kinetic energy $E_{c.m.} - V_C$ available at the lower bombarding energy. However, it is surprising that this energy limit, calculated assuming spherical nuclei and indicated by the horizontal arrows, does not show up more distinctly in the experimental data. This fact can again be interpreted as an indication of a strong dynamical deformation of the system, evolving continuously with increasing interaction time.

The dominant role of the energy-loss parameter is made obvious by Fig. 14, where the full width at half maximum FWHM of the charge distributions

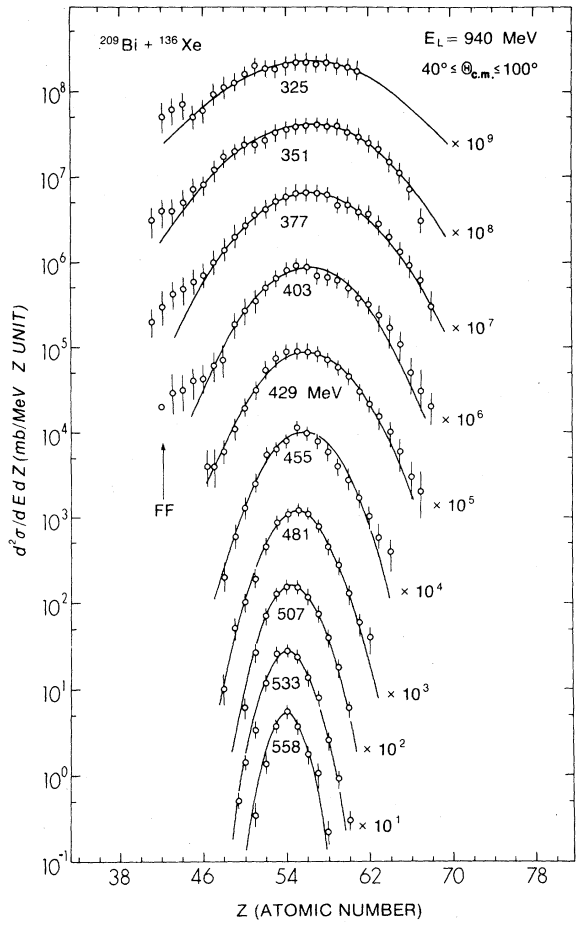

FIG. 12. Fragment Z distributions plotted as a function of the total kinetic energy indicated at the curves. The TKE bins are 26 MeV wide. The curves represent Gaussian fits. The distribution at the bottom corresponds to elastically scattered Xe ions and illustrates the experimental Z resolution. The arrow labeled FF indicates contamination with sequential fission of target-like fragments.

is plotted as a function of energy loss and scattering angle. The horizontal lines represent the fits to the angle-integrated data as shown in Fig. 12. It is obvious that there is no correlation between the scattering angle and the width of the charge distribution for any given energy loss.

Figure 15 shows the contour lines of $d^3\sigma/dZ\,d\Omega\,dE$ in a series of Wilczyński plots for 3-Z-unit-wide bins. Since the statistical accuracy of triple-differential cross sections is not very high, one has to assign large uncertainties to the contour lines, especially for the Z bins far away from Xe. As can be seen from Fig. 15, positive and negative charge transfers lead to approximately the same shape of the Wilczyński plot. However, a slight influence of the Coulomb barrier calculated for spherical systems may be seen in the fact that the center of the distributions for large positive charge transfers ($\Delta Z > 6$) is systematically at higher TKE values than for the corresponding negative charge transfers. In addition, the total cross sections for the positive charge transfer is systematically somewhat higher because the Z distribution is slightly skewed to large Z values (Fig. 5) due to the weak drift towards charge equilibrium.

IV. IMPLICATIONS OF THE BOMBARDING-ENERGY DEPENDENCE FOR THE REACTION MECHANISM OF STRONGLY DAMPED COLLISIONS

A. Correlations between total kinetic energy loss and mass diffusion

The understanding of the mechanism of strongly damped collisions of a few MeV/u has progressed to a stage where the gross features of the reaction are well established. Strongly damped collisions are basically binary processes, where the orbital angular momentum l_i in the entrance channel is the governing parameter for the evolution of a particular collision.

The mean values of the kinematic observables for a given l_i (such as scattering angle, energy loss, and angular momentum) follow the laws of classical mechanics assuming conservative potentials and phenomenological friction forces.[12,14,15] The second moments of the observables can be described in terms of quantal[15,16] and statistical fluctuations,[17] the latter ones arising from the exchange of nucleons between the two colliding nuclei. This microscopic flux of nucleons, responsible for the observed charge and mass transfer, can also account for a considerable fraction of the observed energy loss because of the momentum transfer[18] by the nucleons crossing the boundary between the moving heavy ions.

The dissipation of kinetic energy by this mechanism may be described by a friction force $\vec{F}$, which in a classical model can be written as

$$\vec{F} = j(2u_r \hat{e}_r + u_t \hat{e}_t)\,, \tag{4.1}$$

where u_r and u_t are the radial and tangential components of the relative velocity $\vec{u}$ of the two colliding nuclei, and j is the one-sided mass flux of exchanged nucleons. For a completely open window of area A permitting an unrestricted flux of particles, j is given by $j = n_0 A$, where $n_0 = \rho\bar{v}/4$ is the static one-sided bulk flux, $\bar{v}$ is the average velocity of nucleons, and ρ is the mass density of nuclear matter. Here and in the following paragraphs it is assumed that the magnitude of $\vec{u}$ is small compared with $\bar{v}$.

TABLE IV. ^{209}Bi + ^{136}Xe at $E_L = 940$ MeV ($E_{c.m.} = 569$ MeV). The first E window is 23 MeV wide, all others 26 MeV. The variance σ_Z^2 is corrected for the experimental Z resolution. The total cross section accounted for amounts to 1.96 b. θ_{max} is the angle where $d\sigma/d\Omega_{c.m.}$ has its maximum in the c.m. system for each E bin.

Bin no.	$\langle E \rangle$ MeV	$\langle E_{loss} \rangle$ MeV	σ_Z^2	$\langle Z \rangle$	$d\sigma/dE$ mb/MeV	θ_{max} deg
12	558	12	0.4 ± 0.2	54 ± 0.1	14.2	64
11	533	35	1.2 ± 0.3	54.3 ± 0.3	10.4	64
10	507	61	2.3 ± 0.4	54.5 ± 0.5	7.1	66
9	481	87	3.6 ± 0.4	55.1 ± 0.5	6.1	67
8	455	113	5.7 ± 0.8	55.6 ± 0.7	6.3	68
7	429	139	9.7 ± 1.5	55.9 ± 0.7	7.2	69
6	403	165	13.0 ± 2.5	56.0 ± 1.0	7.8	70
5	377	191	19.9 ± 3.3	56.3 ± 1.0	7.1	72
4	351	217	29 ± 7	56.8 ± 1.0	5.2	72
3	325	243	39 ± 15	57.0 ± 1.5	3.1	76
2	299	269			1.7	76
1	273	295			0.9	

The exchange of nucleons gives rise to a finite width of the mass and charge distribution due to the statistical nature of this exchange. The random-walk theory relates the variance σ_A^2 of the mass distribution to the total number N of exchanged nucleons by

$$\sigma_A^2 = N, \tag{4.2}$$

where N is given by the time integral of the total particle flux (left and right) $2j/m$ integrated over the interaction time τ associated with the collision. In the same way, the total energy loss is given by a time integral of the kinetic energy-loss rate $-dT/dt$:

$$E_{loss} = -\int_0^\tau \frac{dT}{dt}\, dt \tag{4.3}$$

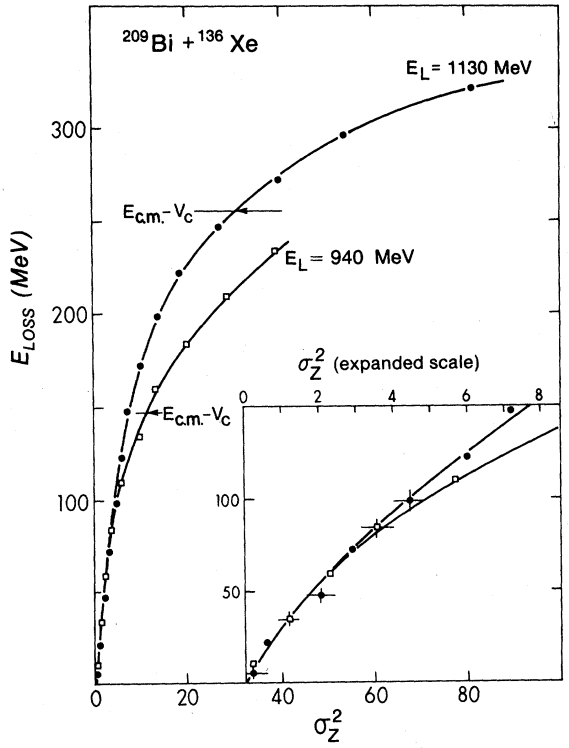

FIG. 13. Experimental correlation between E_{loss} and the variance σ_Z^2 of the fragment charge distribution for two bombarding energies. The insert shows the same data on a larger scale.

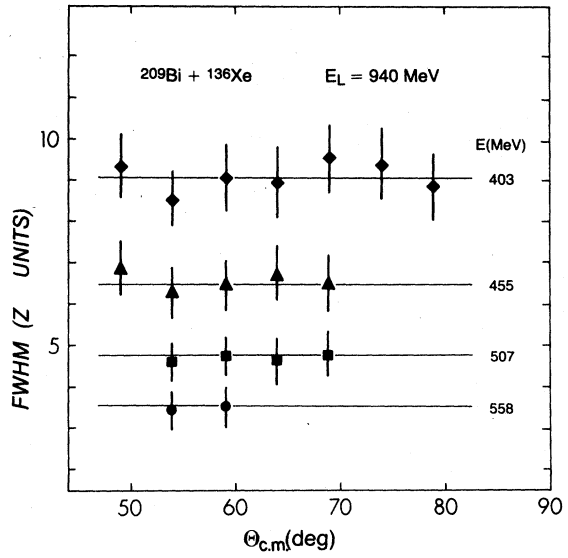

FIG. 14. The width (FWHM) of the fragment Z distribution is plotted versus the reaction angle for various bins of the total kinetic energy. The horizontal lines represent fits to the angle-integrated Z distributions as shown in Table IV.

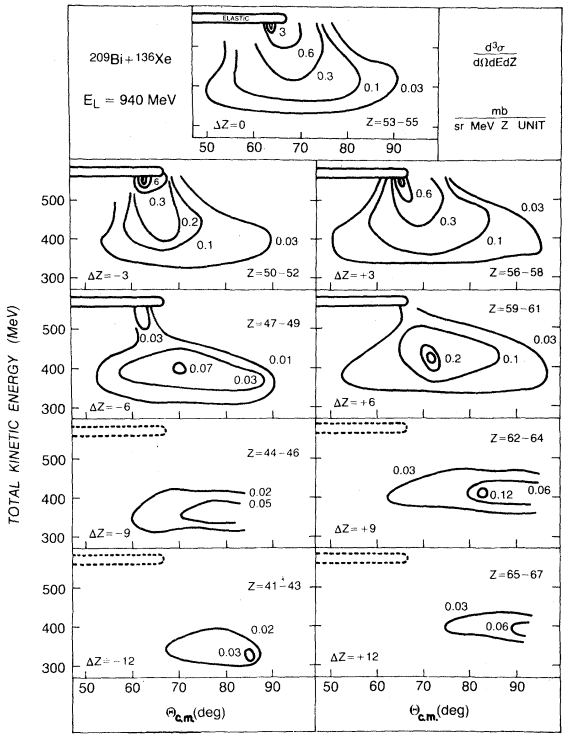

FIG. 15. Triple-differential cross sections $d^3\sigma/dZd\Omega dE$ plotted as contour diagrams with the atomic number of the fragment as parameter. $\Delta Z = Z - 54$ is the difference between the centroid of each Z bin and the atomic number of Xenon.

with

$$\frac{-dT}{dt} = \vec{F}(t)\,\vec{u}(t) = j(t)(2u_r^2 + u_t^2),$$

where $T = \frac{1}{2}\mu\,\vec{u}^2$ is the instantaneous kinetic energy of the relative motion of the nuclei in the center-of-mass system and $\vec{F}(t)$ is the friction force defined in Eq. (4.1). For peripheral reactions the radial component of the velocity $\vec{u}$ is much smaller than the tangential component. Thus one may neglect u_r and write

$$\frac{dT}{dt} = -j(t)\,u_t^2 = -j(t)\frac{2}{\mu}\,T(t). \tag{4.4}$$

Differentiating Eq. (4.2) with respect to t gives

$$\frac{dN}{dt} = \frac{d\sigma_A^2}{dt} = \frac{2j(t)}{m}. \tag{4.5}$$

Thus one can express dt in terms of $d\sigma_A^2$, as has been suggested by Schröder *et al.*[1]

Inserting Eq. (4.5) into Eq. (4.4) results in the differential equation

$$\frac{dT(t)}{T(t)} = -\frac{m}{\mu}\,d\sigma_A^2 = -\frac{m}{\mu}\left(\frac{A}{Z}\right)^x d\sigma_Z^2, \tag{4.6}$$

where the mass and charge variances have been related by

$$\sigma_A^2 = \left(\frac{A}{Z}\right)^x \sigma_Z^2. \tag{4.7}$$

Here, $x = 1$ and $x = 2$ represent the extreme assumptions of totally uncorrelated and totally correlated proton and neutron exchange,[19] respectively. These terms refer to the distribution of reaction products in the N-Z plane. The contour lines of constant cross section are circles in the former and straight lines in the latter case.

The solution of the differential equation (4.6) is given by

$$\ln(T_0/T) = \frac{m}{\mu}\left(\frac{A}{Z}\right)^x \sigma_Z^2, \tag{4.8}$$

where $T_0 = E_{\text{c.m.}} - V_c$ and $T = E_{\text{c.m.}} - V_c - E_{\text{loss}}$ are the kinetic energies in the entrance and exit channels. Thus this model predicts a linear relationship between $\ln(T_0/T)$ and σ_Z^2, with a slope given by $(m/\mu)(A/Z)^x$. In Fig. 16 the experimental data are shown for the reaction at 940 and 1130 MeV. It is seen that the data indeed follow straight lines for both bombarding energies and not too high energy losses. This experimental observation may be regarded as an indication for energy dissipation and the proton exchange to be of statistical nature and to occur on the same time scale. The above simple classical model, however, fails to explain the observed bombarding-energy dependence of the slope, and the value for the slope as given by Eq. (4.8) is too small compared to the experimental results, as can be seen from Table V. It has been sug-

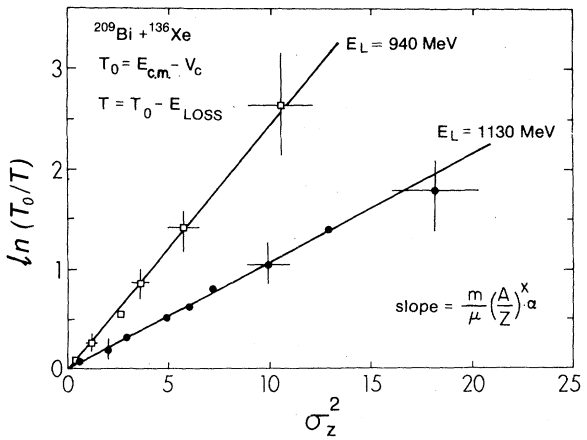

FIG. 16. The variance σ_Z^2 of the charge distribution is plotted versus the logarithm of the ratio T_0/T of the available kinetic energy in the entrance and exit channel. The slope of the resulting linear dependence is a measure for the contribution of the momentum transfer by nucleon exchange to the total observed kinetic energy loss.

TABLE V. Comparison of experimental and theoretical slopes $(m/\mu)(A/Z)^x\alpha$ from the linear relation of $\ln(T/T_0)$ vs σ_Z^2 for the $^{209}Bi + ^{136}Xe$ reaction at bombarding energies of 940 and 1130 MeV. This slope is a measure of the fraction of energy loss associated with nucleon exchange. The quantity μ/m is the reduced mass number of the dinuclear system $T_0 = E_{c.m.} - V_C$ and $T = E_{c.m.} - V_C - E_{loss}$. The values of $x=1$ and $x=2$ represent extreme assumptions of uncorrelated and correlated proton and neutron exchange, respectively. For the classical model $\alpha = 1$ [see Eq. (4.8)]. For the quantal model (see text) α is calculated approximately by Eq. (4.9) and always has a numerical value larger than one.

E_{lab} (MeV)	Experimental slope (see Fig. 16)	Classical slope $x=1$	Classical slope $x=2$	Quantal slope $x=1$	Quantal slope $x=2$
940	0.25	0.03	0.08	0.09	0.23
1130	0.11	0.03	0.08	0.07	0.17

gested by Randrup[18,20] and Schröder *et al.*[21] that the effect of the Pauli principle plays an important role in the calculation of nucleon exchange. Only those nucleons close to the Fermi surface can participate in the exchange, and thus the flux of nucleons through the window is reduced by a factor $1/\alpha$ as compared to the classical value. Accordingly, the variance σ_A^2 of the mass distribution, which is given by Eq. (4.2), is reduced by the Pauli principle. It can be proven,[21] however, that the total energy-loss rate is not affected by the reduction of the flux, since each transferred nucleon carries on the average a larger amount of momentum than in the classical case, since only fast nucleons close to the Fermi surface can be exchanged. It has been shown[18] that drift coefficients including both the rate of energy loss and the net mass transfer are not affected by the inclusion of the Pauli principle in a theory which is based on one-body transition operators.

Since the quantum-mechanical treatment leads to a variance σ_A^2 that is smaller than the value expected classically, but does not affect the energy-loss rate, the classical expression for the slope has to be multiplied with the factor α to account for the quantum-mechanical reduction of the nucleon flux. Moreover, the importance of the Pauli blocking is expected to depend strongly on the relative velocity of the two ions, since the relative momentum displaces the Fermi momentum spheres of the two nuclei in k space and opens up otherwise inaccessible parts of the phase space, thus reducing the impact of the Pauli principle on the mass dispersion for higher bombarding energies. Therefore, the slope for a bombarding energy of 1130 MeV is predicted to be smaller than for 940 MeV, in accordance with experiment. A more quantitative comparison of the quantal theory with experimental data has to await a complete dynamical calculation taking into account the velocity-dependent blocking and has, in addition, to account for the correlation between neutron and proton exchange.

An estimation of the reduction of the flux, however, can be made by considering the displacement of two Fermi spheres of equal radius k_F by the momentum k, corresponding to the relative motion of the two nuclei. If one assumes $k_F \gg k$, a simple geometrical calculation of the ratio α of the total volume occupied by nucleons in k space to that where the two spheres do not overlap yields the relation

$$\alpha = \frac{2}{3}\frac{k_F}{k} = \frac{2}{3}\left(\frac{\mu T_F}{m(E_{c.m.} - V_c)}\right)^{1/2}. \qquad (4.9)$$

Here $T_F = 37$ MeV is the Fermi kinetic energy in nuclear matter and μ/m is the reduced mass number of the dinuclear system. Since nucleon exchange is restricted to those parts of phase space where the two Fermi spheres do not overlap, Eq. (4.9) gives approximately the reduction of the flux from its classical value and, therefore, also the increase of the slope as compared to Eq. (4.8). Inserting the parameters from Table I for the 940 and 1130 MeV experiments into Eq. (4.9), one obtains theoretical values of $\alpha = 3.0$ and 2.3, respectively. In Table V, the experimental values for the slopes are compared to the predicted ones, assuming either totally correlated or uncorrelated nucleon exchange. It can be seen from this comparison that the assumption of correlated nucleon exchange [i.e., $\sigma_A^2 = (A/Z)^2\sigma_Z^2$] and introduction of Pauli blocking leads to a reasonable agreement with the experimental data. This simple calculation of the blocking, however, leads to a bombarding-energy dependence of α that is too weak compared to the data. For a more realistic calculation, such effects as the variation of the wave number along a trajectory, the influence of a nonzero nuclear temperature and of the driving forces in the A-Z plane have to be included. It was the aim of this discussion, however, to demonstrate that the experimental data indicate the importance of Pauli blocking in nucleon exchange processes.[22] In addition, it should be pointed out that further simultaneous measurements of the mass and charge distributions would be very helpful to disentangle the effects of the proton-neutron correlations from those due to the Pauli blocking on the function $\sigma_Z^2(E_{loss})$. Only then will it be possible to decide whether the nucleon exchange process alone can account for the large energy losses observed

or if additional energy dissipation mechanisms such as shape degrees of freedom have to be included. A recent experimental study[23] of the reaction $^{208}Pb + ^{136}Xe$ at a very low bombarding energy ($E_{c.m.} - V_c \approx 40$ MeV) indicates that for this system the correlation between σ_A^2 and σ_Z^2 is given by the correlated limit ($\chi = 2$). If this result holds also for the system $^{209}Bi + ^{136}Xe$ at the higher bombarding energies studied here, then most of the observed energy loss up to 150 MeV can be accounted for by the nucleon exchange mechanism. This point will be further discussed in Sec. IV C.

B. Angular momentum decomposition

A procedure described in Ref. 1 was used to extract an angular momentum scale from the data. For this purpose, a monotonic relationship between the angular momentum in the entrance channel and the total kinetic energy loss was assumed, neglecting fluctuations predicted[24] to be of particular importance for central collisions. Using the relation

$$\frac{d\sigma}{dl} = \pi \lambda^2 (2l+1) T_l \qquad (4.10)$$

between cross section and angular momentum, a one-to-one relationship between the experimental energy-loss spectrum $d\sigma/dE_{loss}$ and $d\sigma/dl$ can be established.[25] The transmission coefficients T_l may be taken either from the sharp-cutoff model or the optical-model fit to the elastic scattering data. In the following analysis the latter were taken. The results of this analysis are shown in Fig. 17 and the first three columns in Table VI. As can be seen, there is a nearly linear relationship between l and E_{loss} for both bombarding energies.

The above l scale is used in conjunction with the angle θ_{max}, giving the location of the cross-section

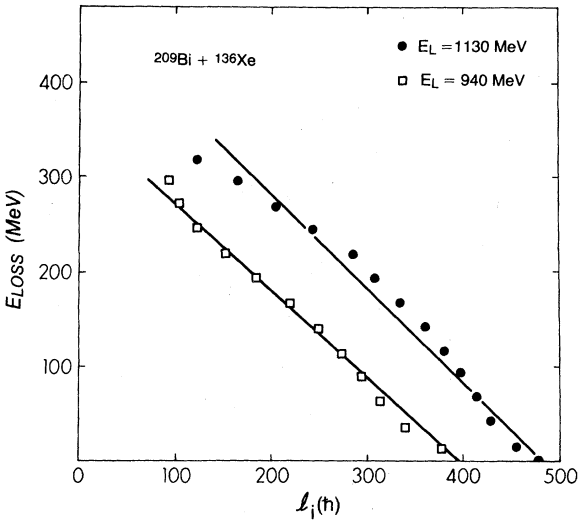

FIG. 17. Correlation between the angular momentum in the entrance channel and the loss of total kinetic energy. The decomposition of the cross section into partial waves assumed a monotonic relation between angular momentum and kinetic energy loss.

maximum (cf. Table IV), to construct an experimental deflection function $\theta(l)$. The results for the two bombarding energies are shown in Fig. 18. As was already obvious from the Wilczyński plot, the ridge of maximum cross section for the 940-MeV data moves to larger scattering angles with decreasing impact parameter, qualitatively similar to a Coulomb deflection function. However, there is still a considerable angle $\Delta\theta$, by which the double-nucleus system rotates to forward angles before it breaks apart,[14] as can be seen from a comparison with the sum θ^c of the Coulomb deflection angles in entrance and exit channels. Details of the calculation can be found in Refs. 1 and 25. The labels NS and S indicate the extreme cases of

TABLE VI. The results of the angular momentum decomposition.

		Nonsticking model				Sticking model			
Bin no.	$\langle E_{loss} \rangle$ MeV	$\langle l_i \rangle$ $\hbar$	$\Delta\theta$ deg	τ 10^{-22} sec	$\bar{D}_Z$ 10^{22} sec^{-1}	$\langle l_f \rangle$ $\hbar$	$\Delta\theta$ deg	τ 10^{-22} sec	$\bar{D}_Z$ 10^{22} sec^{-1}
12	12	376	7.5	1.2	0.17	288	14.9	3.8	0.05
11	35	340	13.6	2.4	0.26	261	21.2	6.0	0.10
10	61	314	16.8	3.1	0.37	241	24.4	7.5	0.15
9	87	294	20.3	4.0	0.44	225	27.9	9.1	0.20
8	113	273	24.4	5.2	0.54	209	31.8	11.2	0.25
7	139	249	29.4	6.9	0.70	191	36.6	14.2	0.34
6	165	219	36.5	9.8	0.67	168	43.1	19.0	0.34
5	191	184	46.9	14.9	0.67	141	52.9	27.7	0.36
4	217	150	60.6	23.7	0.61	115	65.7	42.2	0.34
3	243	122	66.4	31.9	0.61	94	70.6	55.8	0.35
2	269	102	73.3	42.1		78	76.8	72.6	
1	295	90				69			

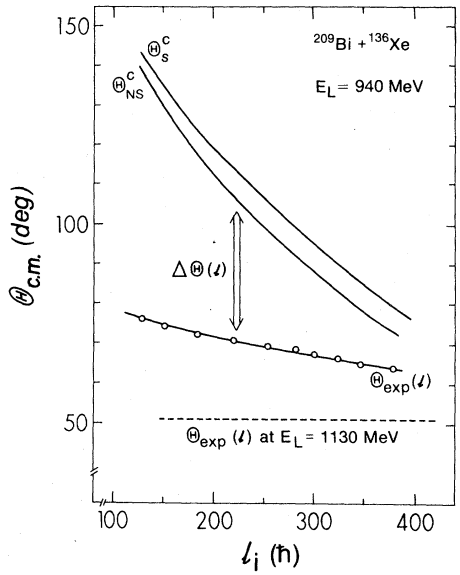

FIG. 18. The average experimental deflection functions for 940 and 1130 MeV is compared to the sum of the Coulomb deflections in the entrance and exit channels for the nonsticking and sticking models at 940-MeV bombarding energy.

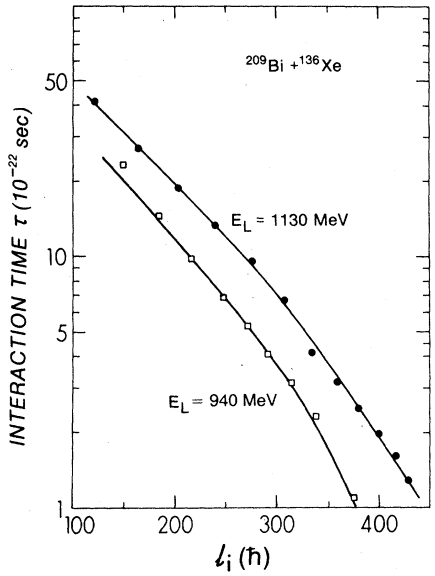

FIG. 19. The angular momentum dependent interaction times for 940- and 1130-MeV bombarding energy.

a nonsticking and sticking contact of the nuclear surfaces during the interaction time. In the latter case 23% of the angular momentum l_i in the entrance channel is converted into intrinsic spin of the colliding nuclei. In the nonsticking case, the final orbital angular momentum l_f is the same as in the entrance channel. The interaction time is calculated as

$$\tau(l_i) = \Delta\theta(l_i)\vartheta(l_i)/\hbar l_f \tag{4.11}$$

and ϑ represents the appropriate moment of inertia for the nonsticking and sticking case, for which the following values were taken:

$$\vartheta_{NS} = \mu R_{int}^2 , \tag{4.12}$$

$$\vartheta_S = \mu R_{int}^2 + \tfrac{2}{5}(M_P R_P^2 + M_T R_T^2) . \tag{4.13}$$

The interaction times thus deduced as a function of l_i are given in columns five and nine of Table VI. The results for the nonsticking model are shown in Fig. 19. At both bombarding energies the interaction times increase approximately exponentially with decreasing orbital momentum. Thus the lifetimes can be parametrized as

$$\tau(l_i) = \begin{cases} 1.53\times10^{-20}\exp(-l_i/80)\,\text{sec}, & E_L = 940\ \text{MeV} \\ 2.18\times10^{-20}\exp(-l_i/84.8)\,\text{sec}, & E_L = 1130\ \text{MeV} . \end{cases} \tag{4.14}$$

As can be seen, the slopes are comparable for both bombarding energies, but for a given l_i the interaction time is about twice as long for the higher bombarding energy. For a given impact parameter, the interaction times are nearly the same for both energies.

C. Classical trajectory calculations

The phenomenological analysis presented in the previous section allowed the extraction of the scattering angle $\theta_{c.m.}$, the total kinetic energy loss E_{loss}, and the interaction time τ as functions of the angular momentum l_i. The same quantities can be obtained as the result of classical dynamical calculations. In the following, a model[26] with four degrees of freedom is discussed. The time-dependent distance r of the centers of the spherical nuclei, the angle θ between the line connecting them and the beam axis, and the angles of rotation θ_T and θ_P of the two spheres were determined by the following equations of motion:

$$\begin{aligned} \mu\ddot{r} &= \frac{-\partial V_C}{\partial r} - \frac{\partial V_N}{\partial r} + \mu r\dot{\theta}^2 - f_r(r)\dot{r} , \\ \mu r^2\dot{\theta} &= l = l_i - J_T - J_P , \\ \dot{J}_T &= -C_T\left(\frac{r}{C_T + C_P}\right)^2 f_\theta(r)[\,C_T(\dot{\theta}_T - \dot{\theta}) + C_P(\dot{\theta}_P - \dot{\theta})\,] , \\ \dot{J}_P &= -C_P\left(\frac{r}{C_T + C_P}\right)^2 f_\theta(r)[\,C_T(\dot{\theta}_T - \dot{\theta}) + C_P(\dot{\theta}_P - \dot{\theta})\,] . \end{aligned} \tag{4.15}$$

Here l_i, J_T, and J_P are the orbital angular momenta in the entrance channel and the spins of the target and projectile, respectively. The quantities μ, C_T, and C_P are the reduced mass of the system and the radii of projectile and target, as taken from Myers' systematics.[27] In order to solve the above equation, the Coulomb potential V_C, the nuclear potential V_N, the radial friction form factor $f_r(r)$, and the tangential friction form factor $f_\theta(r)$ have to be specified. The Coulomb potential proposed by Bondorf, Sobel, and Sperber[14] for heavy ions was taken for all calculations. For the nuclear potential, the proximity potential,[28] a modified version of the proximity potential,[20] and the Krappe-Nix potential[12] were chosen. In the modified version of the proximity potential derived from the consideration that the maximum nuclear density is limited to the nuclear bulk value, the repulsive hard core of the normal proximity potential is absent. The proximity potentials were used in conjunction with the proximity friction force given by Randrup,[18] which is essentially due to the mechanism described in Eq. (4.1). The Gross friction force[12] with radial and tangential strength parameters of $k_r = 2.5 \times 10^{-26}$ and $k_t = 10^{-28}$ sec fm^2 MeV^{-3} was used in connection with the Krappe-Nix potential.

Figure 20 shows the results of the classical calculations solving Eqs. (4.15) in comparison with the data (full symbols) obtained from the partial-wave analysis. The lowest part of Fig. 20 depicts the deflection function. The general trend of a Coulomb-dominated behavior is reproduced about correctly, but the theoretical calculations show too much structure due to the Coulomb and nuclear rainbows, and the modified proximity potential leads to fusion for $l_i < 150$, which appears to be unphysical.

The uppermost part of Fig. 20 shows the interaction times as a function of l_i. Here the interaction time in the calculation is defined as that period of time where the distance between the centers of the two is smaller than the interaction radius. The calculations using the soft proximity and the Krappe-Nix potentials qualitatively reproduce the results of the phenomenological analysis, whereas the hard core of the standard proximity potentials yields much shorter interaction times for $l_i < 250$.

The middle part of Fig. 20 shows E_{loss} as a function of l_i. It is obvious that all three calculations fail to reproduce the large energy losses observed. To a large extent this is due to the fact that no shape degrees of freedom were incorporated into the calculations, so that the available energy above the Coulomb barrier is an upper limit for the energy which can be dissipated. The importance of deformations is demonstrated by the fact that events with a total kinetic energy as low

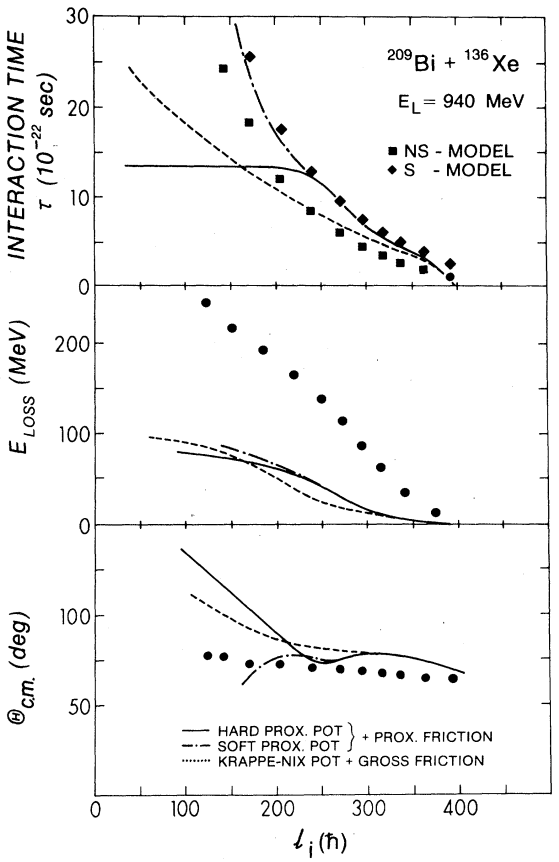

FIG. 20. The experimentally deduced deflection function, total kinetic energy loss, and interaction time as a function of the angular momentum are compared to classical trajectory calculations, using potential and friction form factors as indicated. No deformations are taken into account.

as 270 MeV have been observed. This energy corresponds to the Coulomb repulsion of two spherical Bi and Xe ions 23.6 fm apart and is close to the lowest E value (280 MeV) observed at 1130 MeV bombarding energy and comparable to the predicted[29] mean kinetic energy (300 MeV) released by fission of a fictitious compound system {Xe +Bi}. This may indicate that the highest energy losses occurring in a strongly damped collision are not determined by the details of the reaction mechanism, but by the same properties of nuclear matter which govern the snapping of the neck in fission.

The importance of surface degrees of freedom (vibrations[30] or forming of a neck[21]) is less obvious for more peripheral collisions. Figure 20 shows that calculations for spherical ions underestimate the energy loss as compared with phenomenological analyses for all l values. Inclusion of a neck degree of freedom strongly enhances the energy loss

even for large impact parameters, but it appears premature to conclude from this comparison that deformations are important for peripheral collisions.

D. Transport coefficients derived from the phenomenological model

In the framework of a diffusion model,[17] the time evolution of an observable x such as the charge transfer $\Delta Z = Z - Z_0$ in the reaction is governed by the Fokker-Planck equation

$$\frac{\partial}{\partial t} P(x,t) = \frac{-\partial}{\partial x}[v_x(x,t)P(x,t)] + \frac{\partial^2}{\partial x^2}[D_x(x,t)P(x,t)], \quad (4.16)$$

where v_x and D_x are the drift and diffusion coefficient, respectively. For constant transport coefficients the solution of Eq. (4.16) is a Gaussian

$$P(x,t) = (4\pi D_x t)^{-1/2} \exp[-(x - v_x t)^2/(4D_x t)], \quad (4.17)$$

where the variance and the centroid of the distribution are given by $\sigma_x^2 = 2D_x t$ and $x_0 = v_x t$, respectively. As discussed in Sec. IV A, however, there is no reason to expect the transport coefficients to be time independent, since the exchange of nucleons certainly depends strongly on the relative distance between the two nuclei. Time-dependent transport coefficients still lead to Gaussian solutions, however, if they do not depend explicitly on the variable x. The experimental Gaussian shape of the Z distributions shown in Fig. 12 indicates, therefore, only that the charge drift coefficient v_z and the diffusion coefficient D_Z are very weakly dependent on the fragment charge Z. The experimentally measured variance can then be written as

$$\sigma_Z^2 = 2\int_0^\tau D_Z(t)dt \equiv 2\bar{D}_Z\tau, \quad (4.18)$$

where a time-averaged diffusion coefficient $\bar{D}_Z$ has been defined by introducing the interaction time τ. Since the latter has been extracted from the data using the phenomenological procedure described in Sec. IV B, it is possible to determine the experimental value of the time-averaged diffusion coefficient $\bar{D}_Z$. Since the interaction time τ as well as the width σ_Z^2 are strongly dependent on the impact parameter, it is expected that these diffusion coefficients are functions of the angular momentum in the entrance channel: $\bar{D}_Z = \bar{D}_Z(l_i)$. Assuming the nonsticking model for the derivation of the interaction times, the two curves shown in Fig. 21 are obtained using Eq. (4.18). For both bombarding energies, the diffusion coefficient rises quickly

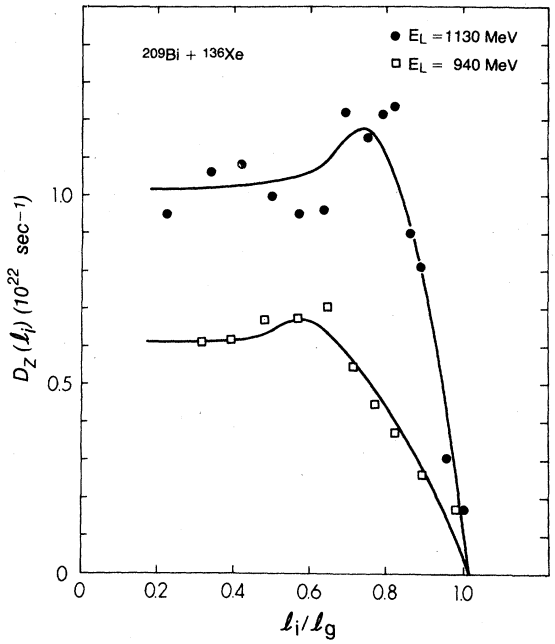

FIG. 21. Average proton number diffusion coefficients $\bar{D}_Z(l_i)$ as a function of the angular momentum for two bombarding energies. The curves are to guide the eye.

with decreasing l for angular momenta close to the grazing l, but reaches a plateau for intermediate and low l values. As has been pointed out in Ref. 1, this behavior might be attributed to the presence of the conservative and radial friction forces, which limit the interpenetration depth of the two colliding ions over a wide range of l values. Thus the size of the window between the ions which largely determines the flux of nucleons and hence the diffusion coefficient remains rather constant for $l < 0.7 l_g$.

The saturation values of the diffusion coefficients D_Z are 1.1×10^{22} sec^{-1} and 0.6×10^{22} sec^{-1} for the high and low bombarding energy, respectively. It is not surprising that for the lower energy D_Z is smaller, since the Pauli blocking of nucleon exchange is more effective and, in addition, the trajectories for a given impact parameter penetrate less deeply, thus reducing the size of the window for nucleon exchange.

An inspection of Fig. 12 shows that the centroids of the charge distributions drift slightly towards symmetry with increasing energy loss. Drift and diffusion coefficients are related by the Einstein relation to the driving force $\partial U/\partial Z$ and the nuclear temperature $\mathcal{T}$:

$$\frac{\Delta Z}{\sigma_Z^2} = \frac{\bar{v}_Z\tau}{2D_Z\tau} = -\frac{1}{2\mathcal{T}}\frac{\partial}{\partial Z}U(Z). \quad (4.19)$$

The model-independent experimental ratio $\Delta Z/\sigma_Z^2$

is approximately constant and equal to 0.21 ± 0.1 for energy losses up to 120 MeV and decreases steadily beyond 120 MeV. If the temperature T is given by the intrinsic temperature of the nucleus,[31] which is related, in a Fermi gas model, to the total excitation energy E^* by

$$aT^2 = E^* \approx E_{\text{loss}} , \tag{4.20}$$

where a is the level density parameter of the combined system, then the magnitude of the right hand side of Eq. (4.19) is large for grazing collisions, which are characterized by a small loss of kinetic energy provided the driving force is not too small. Therefore, a very fast, nondiffusive energy-loss mechanism has been postulated[32] which would heat the system to a high temperature before the diffusion starts and thus explain the experimentally observed small drift.

The inclusion of the Pauli principle in the description of the nucleon exchange processes, however, gives a better account of the experimental ratios $\Delta Z/\sigma_Z^2$, without the necessity to introduce additional dissipation mechanisms. The quantum-mechanical treatment[20] reveals that the quantity T entering in Eq. (4.19) is merely a measure of the phase space available for nucleon exchange and equal to the nuclear temperature only in a certain limit. As has been discussed in Sec. IV A, the relative motion of the colliding nuclei opens otherwise inaccessible parts of the phase space and has, therefore, similar effects as a nonzero temperature. To estimate which intrinsic temperature T^* is equivalent to a given relative momentum k, one may assume that a spherical shell of thickness $2T^*$ and mean radius k_F with $T_F = \hbar^2 k_F^2/2$ m contributes to nucleon exchange between two hot nuclei at rest. This shell has a thickness $\Delta k = k_1 - k_2$ in k space related to $2T^*$ by

$$2T^* = \frac{\hbar^2}{2m}(k_1^2 - k_2^2) = \frac{\hbar^2 k_F}{m}\Delta k . \tag{4.21}$$

The ratio of the volume of this shell to the total volume is equated to $1/\alpha$, where α is determined by Eq. (4.9), giving

$$\frac{4\pi k_F^2 \Delta k}{4\pi k_F^3/3} = \frac{3}{2}\frac{k}{k_F} \tag{4.22}$$

and yielding $\Delta k = \frac{1}{2}k$. Inserting Δk into Eq. (4.21) defines an "effective temperature" T^* for intrinsically cold nuclei colliding with a relative momentum k per nucleon:

$$T^* = \frac{\hbar^2}{4m} k k_F = \frac{1}{2}\left[\frac{m(E_{\text{c.m.}} - V_C)}{\mu} T_F\right]^{1/2} . \tag{4.23}$$

Inserting the parameters of Table I yields an effective temperature of 4.1 MeV for the present experiment (940 MeV) in the limit of grazing collisions. A calculation using the model by Randrup[20] leads to the same value.

In order to compare this result with the experiment, it is necessary to obtain an estimate of the static driving force $\partial U/\partial Z$. It can be calculated for spherical nuclei approximately from the liquid-drop masses of the two fragments and the Coulomb, centrifugal, and nuclear potentials. Evaluating the total potential at the strong-absorption radius for grazing collisions yields a driving force of about -1 MeV/Z unit, depending somewhat on the details of the calculation. Inserting this value and the effective temperature into Eq. (4.19), one obtains a theoretical value of 0.14 for $\Delta Z/\sigma_Z^2$. This value is in qualitative agreement with the experiment; therefore, the inclusion of the Pauli principle readily explains the low value of the drift measured in these experiments without the necessity of introducing an additional energy loss mechanism.

It should be noted that nucleon exchange is a fast mechanism in the sense that most of the energy loss associated with nucleon exchange happens during the approach phase of the reaction, where the relative momentum k is high and therefore the energy-loss rate is large. Thus there is less of a qualitative discrepancy between models with high initial energy loss, such as the one proposed by Gross *et al.*,[12] and the diffusion model than is frequently assumed.

V. YIELD OF SUBSEQUENT FISSION

As has been discussed in Sec. III C, there is evidence for sequential fission of the excited Bi-like fragments in approximately 30% ($f = 0.30$) of all nonelastic events. In the following section, a simple formalism will be discussed which allows this fraction to be calculated using known fission properties of heavy elements. The basis of the formalism is a study of the energy dependence of the ratio of neutron to fission width, Γ_n/Γ_f. Assuming the evaporation model description for Γ_n and the Bohr-Wheeler formula for Γ_f,[33] and adopting a Fermi gas expression for the level densities entering these models, one obtains the following expression for the excitation energy dependence of Γ_n/Γ_f:

$$\frac{\Gamma_n}{\Gamma_f} = \frac{4A^{2/3}a_f(E^* - B_n)}{k_0 a_n (2a_f^{1/2}(E^* - E_f)^{1/2} - 1)} \times \exp[2a_n^{1/2}(E^* - B_n)^{1/2} - 2a_f^{1/2}(E^* - E_f)^{1/2}] , \tag{5.1}$$

where $k_0 = \hbar^2/2mr_0^2 \simeq 9.8$ MeV, B_n is the neutron binding energy, E_f is the effective fission barrier, a_n the level density parameter at equilibrium, and a_f is the level density parameter at the saddle

point. Using a compilation[33] of values for B_n, E_f, and a_n/a_f as measured for low excitation energies E^* for 15 nuclei between Lu and U, it is possible to extrapolate Γ_n/Γ_f to the high excitation energies observed in strongly damped collisions.

Since Γ_f/Γ_n shows a very steep, exponential dependence on the excitation energy, it is possible to associate with the condition $\Gamma_n=\Gamma_f$ a critical excitation energy E^*_{cr}, constituting a rather sharp boundary between the regimes of deexcitation by neutron emission and by fission. In Fig. 22 calculated values of E^*_{cr} are plotted as open circles versus the atomic number Z. An approximately linear relationship between E^*_{cr} and Z results, given by

$$E^*_{cr}(Z)=\begin{cases}808-8.9^*Z \text{ MeV}, & Z<91\\ 6 \text{ MeV}, & Z\geq 91 .\end{cases} \tag{5.2}$$

The filled rhomboids indicate measured values for E_{crit}.[34-36] It can be seen that there is good agreement between the existing measurements and the extrapolations. In deducing Eq. (5.2) the dependence of E^*_{cr} on A has been removed by averaging over the broad isotropic distribution of a given element produced in a strongly damped collision.

The effect of angular momentum on the fission probability can be taken into account by renormalizing the values of $E^*_{cr}(Z)$ for the angular-momentum-dependent fission barrier and neutron binding energy.[33] Hence, the inclusion of a nuclear angular momentum J leads to a modification of Eq. (5.2), where the critical energy E^*_{cr} now depends on both Z and J.

$$E^*_{cr}(Z,J)=\begin{cases}E^*_{cr}(Z)(1-J^2/6400), & J\leq 80\hbar\\ 0, & J>80\hbar .\end{cases} \tag{5.3}$$

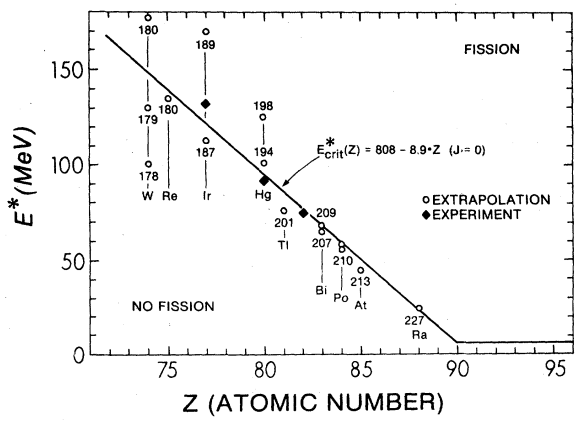

FIG. 22. A systematic relationship between the atomic number Z and excitation energy E^*, where fission width Γ_f and neutron width Γ_n are equal. The straight line is a fit to the data and separates the $Z-E^*$ plane into the domains of deexcitation by neutron emission and by fission, respectively.

Alternatively, Eq. (5.3) can be interpreted as a definition of a critical atomic number $Z_{cr}(E^*,J)$ for each given excitation energy and spin, such that all elements with $Z>Z_{cr}$ decay by fission.

From the measured charge distribution of the Xe-like fragments the distribution of the heavy fragments can easily be deduced assuming that charged-particle evaporation is not an important process. Thus the centroid of the heavy fragment-Z distribution is given by

$$\langle Z\rangle_H = Z_T + Z_p - \langle Z\rangle_L \tag{5.4}$$

and the variances σ_Z^2 corresponding to heavy and light fragments are equal.

In addition, assuming a model for the relation between E_{loss} and the amount of angular momentum transferred into intrinsic spin—such as the nonsticking or sticking models—the two-dimensional surface $Z_{cr}(E^*,J)$ can be reduced to a one-dimensional function $Z_{cr}(E^*)$. The excitation energy E^* can be obtained from E_{loss}, since the division of the available excitation energy occurs approximately proportional to the masses of the fragments.[31,37] For a Gaussian charge distribution, the cross section $\sigma_{SF}(E^*)$ for sequential fission can then be calculated by integrating the charge distribution from $Z_{cr}(E^*)$ upwards:

$$\Delta\sigma_{SF}(E^*)=\frac{\Delta\sigma_R(E^*)}{\sigma_Z(E^*)\sqrt{2\pi}} \times\int_{Z_{cr}(E^*)}^{\infty}\exp\left(\frac{-[Z-\langle Z\rangle_H(E^*)]^2}{2\sigma_Z^2}\right)dZ . \tag{5.5}$$

In Eq. (5.5) $\Delta\sigma_R(E^*)$ is the reaction cross section for a particular E bin. The total probability f for sequential fission is obtained by summing $\Delta\sigma_{SF}$ for all excitation energies. The results are compiled in Table VII for the nonsticking model and for a more realistic J distribution where $J(l_i)$ was parametrized by

$$J(l_i)=J_0(l_i)\left(1+\exp\frac{l_i-l_0}{A}\right)^{-1} \tag{5.6}$$

TABLE VII. Probability $f=\sigma_{SF}/\sigma_R$ for sequential fission of the heavy (Bi-like) fragments.

Bombarding energy (MeV)	940	1130
Experiment	0.30 ± 0.15	
NS model	0.32	0.53
Realistic J distribution	0.37	
NS model and charged particle evaporation	0.27	0.49

and

$$J_0(l_i) = l_i\left(1 - \frac{\vartheta_{NS}}{\vartheta_S}\right)\vartheta_T(\vartheta_T + \vartheta_p)^{-1}. \quad (5.7)$$

Here, J_0 is the spin transfer to the heavy fragment in the sticking limit, and values of $l_0 = 283$ and $A = 45$ were estimated from Ref. 30.

The effect of charged-particle evaporation was studied by reducing $\langle Z\rangle_H$ arbitrarily by one Z unit before integrating Eq. (5.5). It was seen that the results are not sensitive to the assumptions entering the calculation, and the theoretical values compare favorably with the experimental result. For the 1130-MeV data sequential fission of the heavy fragments is predicted to occur with about 50% probability. In Fig. 23 the cross section $d\sigma_{SF}/dE_{loss}$ is shown for sequential fission as a function of E_{loss} for the 940-MeV data as calculated from Eq. (5.5).

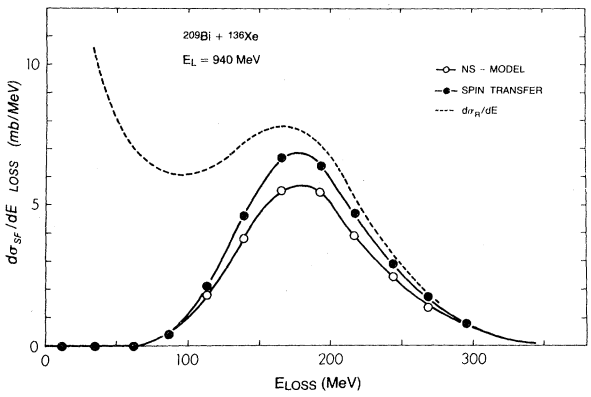

FIG. 23. The calculated cross section $d\sigma_{SF}/dE$ for sequential fission of the heavy-Bi-like fragment as a function of the total kinetic energy loss at 940-MeV bombarding energy. The broken curve indicates the total reaction cross section $d\sigma_R/dE$, as deduced from the Xe-like fragments.

VI. CONCLUSIONS

The study of the reaction ^{209}Bi + ^{136}Xe at a bombarding energy of $E_{lab} = 940$ MeV allowed, in connection with a previous experiment performed at $E_{lab} = 1130$ MeV, a detailed investigation of the bombarding-energy dependence of strongly damped reactions and, in addition, confirmed conclusions drawn from the previous experiment. The angular distribution of the reaction products is characteristic for a fast peripheral process and is strongly dominated by the repulsive Coulomb force, although a considerable rotation of the dinuclear system is observable.

The element distributions of the reaction products for different energy losses are Gaussian and consistent with a diffusion model employing diffusion coefficients that are independent of the atomic number Z. These diffusion coefficients are dependent on the impact parameter for grazing collisions and constant for more central collisions.

The study of the relation between the dissipation of kinetic energy and the width of the charge distribution as a function of the bombarding energy indicates that a classical description of nucleon exchange is not valid. Instead, consideration of the blocking of the nuclear orbitals available for nucleon transfer due to the Pauli principle is essential for an understanding of this relationship as well as of the ratio between charge drift and diffusion. In a simple model, the degree of blocking is inversely proportional to the momentum per nucleon of the relative motion and thus most effective for collisions at low bombarding energies. Further, more refined dynamical calculations including this blocking effect will be necessary to understand quantitatively the experimental results and to decide whether or not energy dissipation due to statistical nucleon exchange can account completely for the large amounts of dissipated energy observed or if additional energy-loss mechanisms have to be included. Further simultaneous measurements of mass and Z distributions at different bombarding energies of selected systems will be helpful because of a strong and characteristic velocity dependence of these processes.

ACKNOWLEDGMENTS

This work was supported by the U. S. Department of Energy. The authors express their gratitude for the hospitality extended to them at the Lawrence Berkeley Laboratory, Berkeley. Particular thanks are due to Dr. M. Zisman for his efficient and continuous support during the experiments and to H. Grunder and the operating staff of the SuperHILAC accelerator. Use of the facilities of the Nuclear Structure Research Laboratory supported by a grant from the National Science Foundation is acknowledged.

[1]W. U. Schröder, J. R. Birkelund, J. R. Huizenga, K. L. Wolf, and V. E. Viola, Jr., Phys. Rep. 45, 301 (1978).
[2]W. U. Schröder and J. R. Huizenga, Annu. Rev. Nucl. Sci. 27, 465 (1977).
[3]J. B. Moulton, J. E. Stephenson, R. P. Schmitt, and G.J. Wozniak, Nucl. Instrum. Methods 157, 325 (1978); H. Essel, P. Sperr, K. Hartel, P. Kienle, H. J. Körner, K. E. Rehm, and W. Wagner (unpublished).

[4]S. B. Kaufman, E. P. Steinberg, B. D. Wilkins, J. Unik, A. J. Gorski, and M. J. Fluss, Nucl. Instrum. Methods 115, 47 (1974).
[5]Recent measurements using 780-MeV Xe ions were consistent with the large pulse-height defect described in Ref. 3.
[6]J. R. Birkelund, J. R. Huizenga, H. Freiesleben, K. L. Wolf, J. P. Unik, and V. E. Viola, Jr., Phys. Rev. C 13, 133 (1976), and references cited therein.
[7]L. C. Northcliffe and R. F. Schilling, Nucl. Data, Sect. A7, 233 (1970).
[8]W. E. Frahn and R. H. Venter, Ann. Phys. (N.Y.) 24, 243 (1963); W. E. Frahn, Phys. Rev. Lett. 26, 568 (1971); Ann. Phys. (N.Y.) 72, 524 (1972).
[9]W. E. Frahn, Nucl. Phys. A302, 267 (1978).
[10]F. G. Perey (unpublished).
[11]C. Olmer, M. Mermaz, H. Buenerd, C. K. Gelbke, D. L. Hendrie, J. Mahoney, D. K. Scott, M. H. Macfarlane, and S. C. Pieper, Phys. Rev. C 18, 205 (1978).
[12]D. H. E. Gross and H. Kalinowski, Phys. Rep. 45, 175 (1978).
[13]J. Wilczyński, Phys. Lett. B47, 484 (1973).
[14]J. P. Bondorf, M. I. Sobel, and D. Sperber, Phys. Rep. C15, 83 (1974).
[15]R. A. Broglia, C. H. Dasso, and Aa. Winther, Phys. Lett. 53B, 301 (1974); H. H. Deubler and K. Dietrich, *ibid.* 56B, 241 (1975); Nucl. Phys. A277, 493 (1977); J. N. De, F. Beck, D. H. E. Gross, and H. Kalinowski, Z. Phys. A277, 385 (1976).
[16]D. Agassi, C. M. Ko, and H. A. Weidenmüller, Ann. Phys. (N.Y.) 107, 140 (1977); 117, 237 (1979); 117, 407 (1979); H. Hofmann and P. J. Siemens, Nucl. Phys. A257, 165 (1976).
[17]W. Nörenberg, Phys. Lett. B52, 289 (1974); Z. Phys. A274, 241 (1976); A276, 84 (1976); S. Ayik, B. Schürmann, and W. Nörenberg, Z. Phys. A277, 299 (1976); A279, 145 (1976); S. Ayik, G. Wolschin, and W. Nörenberg, *ibid.* A286, 271 (1978); C. Riedel, G. Wolschin, and W. Nörenberg, *ibid.* A290, 47 (1979).
[18]J. Randrup, Ann. Phys. (N.Y.) 112, 356 (1978); J. Błocki, Y. Boneh, J. R. Nix, J. Randrup, M. Robel, A. J. Sierk, and W. J. Swiatecki, *ibid.* 113, 330 (1978).
[19]F. Beck, M. Dworzecka, and H. Feldmeier, Z. Phys. A289, 113 (1978); Y. Eyal, G. Rudolf, I. Rode, and H. Stelzer, Phys. Rev. Lett. 42, 826 (1979); J. Barrette, P. Braun-Munzinger, C. K. Gelbke, H. L. Harney, H. E. Wegner, B. Zeidman, K. D. Hildenbrand, and U. Lynen, Nucl. Phys. A299, 147 (1978); P. Braun-Munzinger and J. Barrette, *ibid.* A299, 161 (1978); B. Gatty, D. Guerreau, M. Lefort, X. Tarrago, J. Galin, B. Cauvin, J. Girard, and H. Nifenecker, *ibid.* A253, 511 (1975); H. Breuer, B. G. Glagola, V. E. Viola, K. L. Wolf, A. C. Mignerey, J. B. Birkelund, D. Hilscher, A. D. Hoover, J. R. Huizenga, W. U. Schröder, W. W. Wilcke, Phys. Rev. Lett. 43, 191 (1979).
[20]J. Randrup, Nucl. Phys. A307, 319 (1978); A327, 490 (1979).
[21]W. U. Schröder, J. R. Birkelund, J. R. Huizenga, W. W. Wilcke, and J. Randrup, Phys. Rev. Lett. 44, 308 (1980).
[22]It should be stressed that the interpolation of the quantity α has changed as compared to Ref. 1. In the purely classical treatment of Ref. 1 the nucleon exchange mechanisms could explain only a fraction of the observed energy loss, and α was introduced to describe the effect of an *ad hoc* postulated nonexchange energy-loss mechanism. Now, with the inclusion of quantal effects the nucleon exchange process is found responsible for the majority or possibly all of the observed energy loss, and α is interpreted as the ratio of the classical to the quantal flux of exchanged nucleons. If future results should indicate that nonexchange processes do contribute to the energy loss, then α would have to be interpreted as the sum of this ratio and the contribution from the nonexchange process.
[23]H. Essel, K. Hartel, W. Henning, P. Kienle, H.J. Körner, K. E. Rehm, P. Sperr, W. Wagner, and H. Spieler, Z. Phys. A289, 265 (1979).
[24]G. Wolschin and W. Nörenberg, Phys. Rev. Lett. 41, 691 (1978); A. Olmi, H. Sann, D. Pelte, Y. Eyal, A. Gobbi, W. Kohl, U. Lynen, G. Rudolf, H. Stelzer, and R. Bock, *ibid.* 41, 688 (1978). A particular model [H. Esbensen *et al.*, Phys. Rev. Lett. 41, 296 (1978)] where the entire energy loss is due to surface vibrations leads to sizable fluctuations even for peripheral collisions.
[25]W. U. Schröder, J. R. Birkelund, J. R. Huizenga, K. L. Wolf, and V. E. Viola, Jr., Phys. Rev. C 16, 623 (1977).
[26]J. R. Birkelund, J. R. Huizenga, J. N. De, and D. Sperber, Phys. Rev. Lett. 40, 1123 (1978).
[27]W. D. Myers, Nucl. Phys. A204, 465 (1973).
[28]J. Błocki, J. Randrup, W. J. Swiatecki, and C. F. Tsang, Ann. Phys. (N.Y.) 105, 427 (1977).
[29]V. E. Viola, Jr., Nucl. Data Sect. A1, 391 (1966).
[30]R. A. Broglia, C. H. Dasso, G. Pollarolo, and A. Winther, Phys. Rev. Lett. 41, 25 (1978).
[31]D. Hilscher, J. R. Birkelund, A. D. Hoover, W. U. Schröder, W. W. Wilcke, J. R. Huizenga, A. Mignerey, K. L. Wolf, H. F. Breuer, and V. E. Viola, Jr., Phys. Rev. C 20, 576 (1979).
[32]C. Ngô, J. Péter, B. Tamain, M. Berlanger, and F. Hanappe, Nucl. Phys. A267, 181 (1976).
[33]R. Vandenbosch and J. R. Huizenga, *Nuclear Fission* (Academic, New York, 1973).
[34]U. Lynen, Y. Civelekoglu, A. Olmi, H. Sann, D. Pelte, A. Gobbi, G. Rudolf, H. Stelzer, and R. Bock, Proceedings of the International Workshop on Gross Properties of Nuclei and Nuclear Excitations VI, Hirschegg, Austria, 1978 [AED Conference Report No. 78-007-001 (unpublished)].
[35]L. G. Moretto, in Proceedings of IPCR Symposium, IPCR Cyclotron Progress Report, Suppl. 6, Hakone, Japan, 1977 (unpublished).
[36]M. Rajagopalan, L. Kowalski, D. Logan, M. Kaplan, J. M. Alexander, M. S. Zisman, and J. M. Miller, Phys. Rev. C 19, 54 (1979).
[37]Y. Eyal, A. Gavron, I. Tserruya, Z. Fraenkel, Y. Eisen, S. Wald, R. Bass, G. R. Gould, G. Kreyling, R. Renfordt, K. Stelzer, R. Zitzmann, A. Gobbi, U. Lynen, H. Stelzer, I. Rode, and R. Bock, Phys. Rev. Lett. 41, 625 (1978).